Inorganic Chemistry

Article

pubs.acs.org/IC

Gd–Sc-Based Mixed-Metal Nitride Cluster Fullerenes: Mutual Influence of the Cage and Cluster Size and the Role of Scandium in the Electronic Structure

Anna L. Svitova,[†] Alexey A. Popov,*[,†,‡] and Lothar Dunsch*[,†]

[†]Department of Electrochemistry and Conducting Polymers, Leibniz Institute of Solid State and Material Research, D-01069 Dresden, Germany

[‡]Chemistry Department, Moscow State University, 119992 Moscow, Russia

Supporting Information

ABSTRACT: The influence of the cage as well as of the cluster size has been studied in Gd–Sc nitride cluster fullerenes, which have been synthesized and isolated for these studies. A series of carbon cages ranging from C_{78} to C_{88} have been synthesized, isolated, and characterized in detail using absorption and vibrational spectroscopy as well as electrochemistry and density functional theory calculations. Gd–Sc mixed-metal cluster fullerenes in carbon cages different from C_{80} were described for the first time. A review of their structures, properties, and stability is given. The synthesis was performed with melamine as an effective solid source of nitrogen, providing high fullerene yield and suppressing empty fullerene formation. Substitution of gadolinium by scandium imposes a noticeable influence on the electronic structure of nitride cluster fullerenes as revealed by electrochemical, spectroscopic, and computational methods.

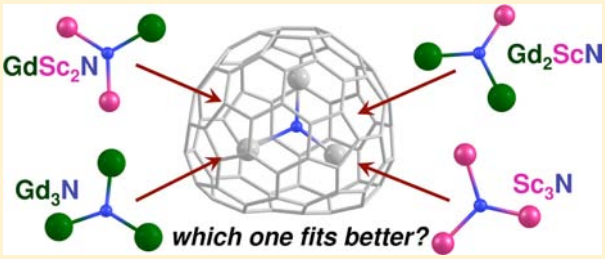

INTRODUCTION

The ability of fullerenes to encapsulate metal atoms in their interior space was first proposed and shown by mass spectrometric analysis by Heath et al.[1] the same year when the fullerenes were discovered. From the time when the existence of the first endohedral fullerenes had been experimentally proven, the world of these new interesting materials and their number have been steadily expanded. However, the low yield of mono- or dimetallic endohedral fullerenes should be taken into account considering their production in an amount sufficient for their detailed analysis or even for commercialization. The discovery of metal nitride cluster fullerenes (NCFs) in 1999,[2] first obtained by introducing a small portion of nitrogen gas into the arc generator during vaporization of graphite rods containing metal oxides, opened the gate for the synthesis of carbon cages with cluster species inside. Neither the trimetallic nitride cluster nor the C_{80} fullerene of icosahedral symmetry has been obtained separately. However, if combined, they can form a new compound with a very high stability and a yield even exceeding that of the C_{84} fullerene.[2] Adding a gaseous (NH_3) or solid organic nitrogen source to the initial materials for the fullerene synthesis significantly enhances the yield of endohedral fullerenes, enabling the formation of macroscopic amounts of highly stable NCFs as the major product of the reaction.[3−5] For this reason, this class of endohedral fullerenes has attracted great attention, and a large number of NCFs, containing homogeneous M_3N or mixed-metal nitride clusters with two $M_xM'_{3-x}N$ or three different metals $M_xM'_yM''_{3-x-y}N$ (M, M′, M″ = metals; x, y = 0−3), entrapped in the fullerene cages of various cage sizes from C_{68} to C_{96}, was obtained and characterized.[6,7] In the past decade, the metals of group III yttrium[8−10] and most of the lanthanides including lanthanum,[11] cerium,[12−14] praseodymium,[13] neodymium,[13,15] gadolinium,[16−22] terbium,[3,23−25] dysprosium,[26−31] holmium,[3,4,32,33] erbium,[2,34] thulium,[35−38] and lutetium,[31,39−42] were encapsulated either inside the carbon cages as M_3N clusters or in the mixed-metal clusters (presumably with scandium).

Among all rare-earth elements, gadolinium is of particular importance because of its special magnetic properties. The Gd ion is a perfect paramagnetic system with seven unpaired electrons and a spherical nature of its ground state ($S = {}^7/_2$; $L = 0$). The organic complexes of Gd^{3+} are currently extensively used as contrast agents for magnetic resonance imaging.[43] Gd^{3+} itself is highly toxic in a free ionic form[44] and, hence, cannot be administrated in the body as it is. In commercial contrast agents, this problem is partially circumvented by the use of organic chelates of gadolinium,[45] albeit some negative effects (e.g., fibrosis in kidneys[46]) still remain. In this regard, the use of Gd-based endohedral fullerenes might have a serious advantage first because the carbon cage keeps Gd ions inside, preventing possible external chemical exposure and the release of Gd^{3+} into the body.[47−50] Second, water-soluble derivatives of Gd-based

Received: January 8, 2013
Published: March 7, 2013

   dx.doi.org/10.1021/ic400049k | Inorg. Chem. 2013, 52, 3368−3380

fullerenes, including Gd-based NCFs, were demonstrated to be more effective contrast agents, exhibiting higher water proton relaxivities in comparison to Gd-based chelates.[51−60] As a consequence of the utility of Gd-NCFs for the design of efficient contrast agents, the persistent interest in these compounds is holding over the past decade.

The metal nitride clusters can be encapsulated in different carbon cages, and the product distribution largely depends on the M^{3+} ionic radius (and, hence, of the M_3N cluster size). For scandium, the main Sc-NCFs are $Sc_3N@C_{68}$, $Sc_3N@C_{78}$, and two isomers with C_{80} cages, of them the $Sc_3N@C_{80}$-I_h being the most abundant endohedral fullerene.[2,6] $Sc_3N@C_{82}$ is the largest Sc-NCF detected by mass spectrometry, although this structure has never been isolated. For lanthanides, a substantial increase in the M^{3+} ionic radius (and, hence, in the M_3N cluster size) results in a shift of the cage distribution to the larger cages. Because of the enhanced stability of the C_{80}^{6-}-I_h cage, the formation of $M_3N@C_{80}$-I_h(7) NCFs is most preferable. At the same time, the limited interior space serves as a natural limitation of the size of the M_3N cluster, which can stabilize the icosahedral C_{80} cage. The radius of Gd^{3+} appears to be a threshold, at which $M_3N@C_{80}$ is still the most abundant Gd-NCF; however, the yields of $Gd_3N@C_{84-88}$ are already comparable (but the overall yield of Gd-NCFs is thus rather low).[17,19,22] Besides, the Gd_3N cluster in $Gd_3N@C_{80}$ is known to be pyramidal,[16] which is an indication of the strong strain induced by the limited cage size. Echegoyen et al. reported that an increase in the metal size beyond gadolinium results in a shift of the most abundant product first toward $M_3N@C_{88}$ (M = Nd) and then to $M_3N@C_{92}$−$M_3N@C_{96}$ (M = La, Ce).[11,13,15] These dramatic changes in the cage distribution are caused by an increase in the M_3N cluster size and increasing strain of $M_3N@C_{2n}$ molecules when larger and larger clusters are encapsulated in the given cage. For lanthanides smaller than gadolinium (e.g., terbium, dysprosium, thulium, lutetium), the distribution of the synthesized NCFs is similar to that of Gd-NCFs except for the higher yield of NCFs in general and the higher relative yield of $M_3N@C_{80}$ in particular. Even for the smallest lanthanide-based cluster Lu_3N, the stepwise increase in the cluster size between Sc_3N and Lu_3N is sufficiently large to cause an abrupt change of the product distribution.

Mixing metals of different sizes in the M_3N cluster enables tuning of the cluster size and, hence, affords the possibility of varying the product distribution in the NCF synthesis. Earlier we have shown that admixing scandium to gadolinium dramatically enhances the yield of Gd-containing fullerenes (the sum yield of $GdSc_2N@C_{80}$ and $Gd_2ScN@C_{80}$ in our conditions is ca. 40 times higher than that of $Gd_3N@C_{80}$ alone)[20] and thus can be fortuitous for practical applications. Furthermore, the Gd−Sc system offers a unique possibility to follow the mutual cluster−cage influence in a much more detailed way than in any homogeneous-metal system. Namely, the availability of the gradually increasing cluster sizes from the "small" Sc_3N via intermediate $GdSc_2N$ and Gd_2ScN to the "large" Gd_3N opens the possibility for carbon cages to adopt the cluster of the most suitable size. In other words, a mixed Gd−Sc system increases the flexibility of the product distribution by providing optimum combinations of the fullerene and cluster sizes for each carbon cage. To address this question, we describe in this work the production, isolation, and spectroscopic and electronic properties of Gd−Sc NCFs, focusing on fullerene cages other than C_{80}.

RESULTS AND DISCUSSION

Synthesis and Isolation of Gd−Sc Mixed-Metal Cluster Fullerenes. As a part of our continuous efforts to increase the yield of NCFs, we have recently established melamine (organic base with the molecular formula $C_3H_6N_6$ and a high nitrogen content of 66% by mass) as a new selective nitrogen source.[61] Gd-containing mixed-metal cluster fullerenes were produced by evaporating graphite rods in the electric arc by the Krätschmer-Huffman method modified in our group.[3,18,20] Matrix-assisted laser desorption ionization time-of-flight (MALDI-TOF) mass spectrometric analysis showed the formation of several mixed-metal NCFs with the general formula $Gd_xSc_{3-x}N@C_{2n}$ (x = 0−3; 39 ≤ n ≤ 44). Analysis of the chromatogram (Figure 1) and

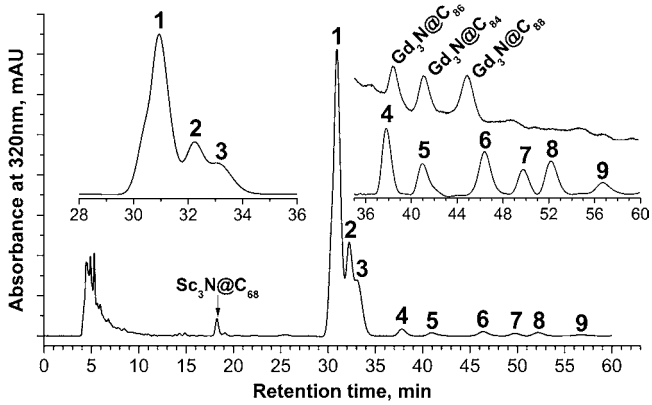

Figure 1. Chromatogram of a $Gd_xSc_{3-x}N@C_{2n}$ fullerene extract mixture synthesized by the arc-discharge method with melamine as a source of nitrogen (HPLC conditions: linear combination of two 4.6 × 250 mm Buckyprep columns; flow rate 1.6 mL min^{-1}; injection volume 200 μL; toluene as the eluent; 40 °C). The right inset shows the enlarged chromatographic region of the fractions containing Gd−Sc mixed-metal NCFs in carbon cages larger than C_{80} compared with the chromatogram of the $Gd_3N@C_{2n}$ extract obtained in the same conditions. The left inset shows expansion of the region of fractions 1−3 containing mainly $Gd_xSc_{3-x}N@C_{80}$.

mass spectra of the obtained fullerene mixture has proven the formation of NCFs as the major products of the reaction, which demonstrates the high selectivity of the synthesis using melamine as a nitrogen source.

Analysis of the peak areas in the chromatogram, which is listed in Table 1, reveals that the yield of the Gd-based products reaches ca. 66% of all synthesized fullerenes. The most abundant fraction eluting with t_{ret} = 29.4−31.8 min mainly consists of $GdSc_2N@C_{80}$(I), $Sc_3N@C_{78}$, and $Gd_2ScN@C_{80}$(I) [here isomers I and II denote I_h(7) and D_{5h}(6) cages]. The relative yield of this fraction determined from the areas of the high-performance liquid chromatography (HPLC) peaks is 63.5%, whereas the yield of $Sc_3N@C_{78}$ is 8.9%. Accordingly, the Gd-containing NCFs $GdSc_2N@C_{80}$(I) and $Gd_2ScN@C_{80}$(I) in the C_{80} carbon cage of icosahedral symmetry are the main products in this synthesis with a relative yield of 54.5%. The second and third major fractions mainly contain $Sc_3N@C_{80}$(I) (16.8%), and the second isomers with the D_{5h}(6) cage $GdSc_2N@C_{80}$(II), $Gd_2ScN@C_{80}$(II), and $Sc_3N@C_{80}$(II) with yields of 4.7%, 2.0%, and 5.5%, respectively, constitute 29% of all fullerene structures formed. Further details of the isolation and spectroscopic studies of $Gd_xSc_{3-x}N@C_{80}$ have been described earlier.[18,20]

dx.doi.org/10.1021/ic400049k | Inorg. Chem. 2013, 52, 3368−3380

Table 1. Gd−Sc Mixed-Metal NCFs Formed by the Arc-Discharge Method with Melamine as the Nitrogen Source and Their Retention Times and Relative Yields Estimated by the Peak Areas in Chromatograms

C_{2n}	M_3N	fraction	retention time,[a] min	yield,[b] %	carbon cage[c]
C_{68}	Sc_3N		18.2	1.6	$D_3(6140)$
C_{76}	$GdSc_2N$	3	32.9−34.5	traces	$\{C_s(17490)\}$[d]
$C_{78}(I)$	Sc_3N	1	29.4−31.8	8.9	$D_{3h}(5)$
	$GdSc_2N$	1	29.4−31.8	traces	$D_{3h}(5)$
$C_{78}(II)$	$GdSc_2N$	5	39.9−42.4	0.6	$C_2(22010)$
$C_{80}(I)$	Sc_3N	2 and 3	31.8−34.5	16.8	$I_h(7)$
	$GdSc_2N$	1	29.4−31.8	43.5	$I_h(7)$
	Gd_2ScN	1	29.4−31.8	11.1	$I_h(7)$
$C_{80}(II)$	Sc_3N	3	32.9−34.5	5.5	$D_{5h}(6)$
	$GdSc_2N$	2−4	31.8−39.1	4.8	$D_{5h}(6)$
	Gd_2ScN	2	31.8−32.9	2.0	$D_{5h}(6)$
C_{82}	Sc_3N	5	39.9−42.4	<0.1	$\{C_{2v}(9)\}$[e]
	$GdSc_2N$, Gd_2ScN	4	36.8−39.1	0.6	$\{C_{2v}(9)\}$[e]
$C_{84}(I)$	$GdSc_2N$	5	39.9−42.4	0.1	$\{D_2(21)\}$[e]
C_{84}	Gd_2ScN	6	45.2−47.9	1.1	$C_s(51365)$
$C_{84}(II)$	$GdSc_2N$	8	51.2−53.5	0.1	$C_s(51365)$
C_{86}	$GdSc_2N$	9	55.6−58.1	0.4	$D_3(17)$
	Gd_2ScN	8	51.2−53.5	1.0	$D_3(17)$
	Gd_3N	4	36.8−39.1	traces	$D_3(17)$
C_{88}	Gd_2ScN	7	48.8−50.9	0.7	$D_2(35)$
	Gd_3N	6	45.2−47.9	<0.1	$D_2(35)$
C_{96}	Gd_3N	8	51.2−53.5	traces	$\{D_2(186)\}$[f]

[a]Retention times are valid for the linear combination of two Buckyprep columns. [b]Yield in percent of total fullerene yield estimated based on HPLC peak areas (detection at 320 nm). [c]Cages with an uncertain assignment are given in curly brackets. [d]Proposed based on ref 27. [e]Proposed based on DFT calculations. [f]Proposed based on refs 62−64.

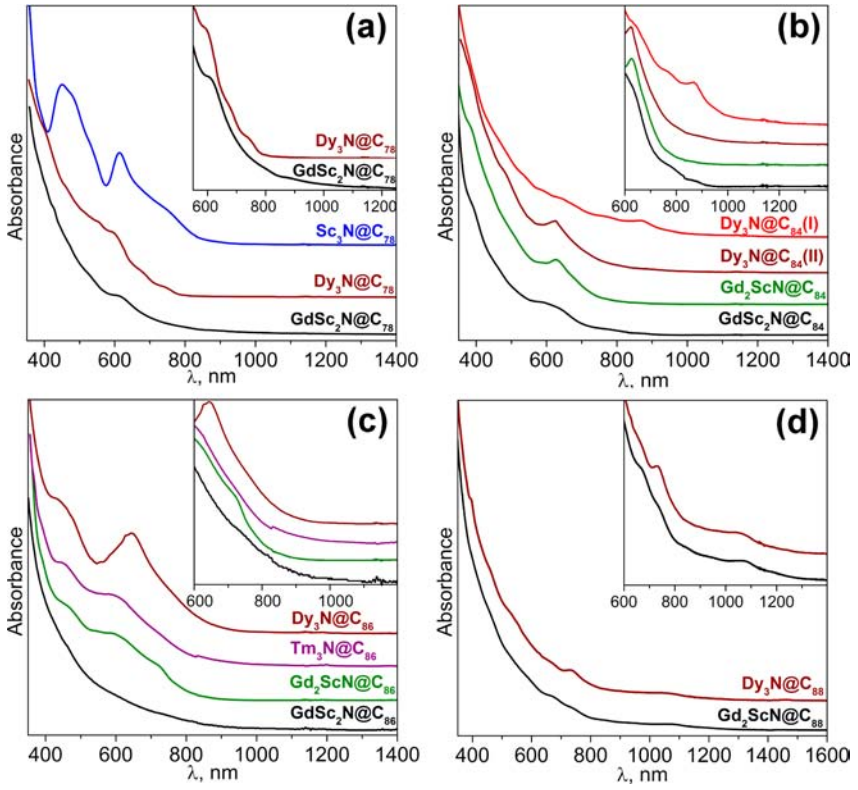

Figure 2. Vis−NIR absorption spectra of $Gd_xSc_{3-x}N@C_{2n}$ NCFs in a toluene solution in comparison to the spectra of other NCFs with the same cage sizes: (a) $GdSc_2N@C_{78}$, $Dy_3N@C_{78}$-$C_2(22010)$ and $Sc_3N@C_{78}$-$D_{3h}(5)$; (b) $GdSc_2N@C_{84}$, $Gd_2ScN@C_{84}$, and two isomers of $Dy_3N@C_{84}$; (c) $GdSc_2N@C_{86}$, $Gd_2ScN@C_{86}$, $Dy_3N@C_{86}$, and $Tm_3N@C_{86}$; (d) $Gd_2ScN@C_{88}$ and $Dy_3N@C_{88}$. The insets show expansion of the low-energy part of the spectra. The spectra of $Dy_3N@C_{2n}$ NCFs are taken from ref 30; that of $Tm_3N@C_{86}$ is from ref 36.

dx.doi.org/10.1021/ic400049k | Inorg. Chem. 2013, 52, 3368−3380

Table 2. Relative Energies and HOMO−LUMO Gaps of $Gd_xSc_{3-x}N@C_{2n}$ [a]

	cluster							
	Sc_3N		$GdSc_2N$		Gd_2ScN		Gd_3N	
cage	ΔE	gap	ΔE	gap	ΔE	gap	ΔE	gap
C_{78}-D_{3h}(5)	0.0	1.26	6.0	1.32	84.1	1.39	116.0	1.24
C_{78}-C_2(22010)	72.8	1.33	0.0	1.41	0.0	1.54	0.0	1.53
C_{80}-I_h(7) [b]	0.0	1.51	0.0	1.56	0.0	1.59	0.0	1.62
C_{80}-D_{5h}(5) [b]	68.8	1.32	60.8	1.34	62.0	1.38	63.1	1.41
C_{82}-C_{2v}(9)	0.0	0.77	0.0	0.91	16.7	0.89	36.5	0.87
C_{82}-C_{2v}(39705)	15.8	1.23	3.6	1.30	0.0	1.37	0.0	1.35
C_{82}-C_s(39663)	15.4	1.48	14.5	1.54	22.8	1.47	26.4	1.54
C_{84}-C_s(51365)			0.0	1.37	0.0	1.42	0.0	1.35
C_{84}-D_2(21)			16.9	1.00	30.5	0.95	41.6	0.93
C_{86}-D_3(17)			0.0	1.31	0.0	1.39	0.0	1.50
C_{88}-D_2(45)			0.0	0.82	0.0	0.86	0.0	1.02

[a] Relative energies (ΔE) are given in kJ/mol; HOMO−LUMO gaps (gap) are in eV. [b] The values are from ref 18.

In addition to C_{80} carbon cages, which are most favorable for different trimetallic NCFs, small amounts of other Gd-containing NCFs were obtained for other cage sizes. The net yield of the latter was estimated to be around 5.4% of all fullerene products. The list of these structures with their retention times, estimated relative yields, and proposed carbon cages is given in Table 1 [see the Supporting Information (SI) for more detailed information on the separation of each fraction by recycling HPLC]. Taking the 1:1 molar ratio of the metals used in the synthesis into account and considering an equal probability of scandium and gadolinium in the M_3N cluster, we can expect a 1:3:3:1 distribution of the Sc_3N:$GdSc_2N$:Gd_2ScN:Gd_3N clusters for each carbon cage. Deviation from this ratio points to the strong influence of the metal size factor. In fact, the 1:3:3:1 distribution has never been found in the whole Sc−Gd system for any cage size. In contrast, the tendency of the metal nitride cluster size to grow with an increase in the carbon cage size is clearly observed for Gd−Sc NCFs in the series from C_{78} to C_{88} carbon cages (for C_{68}, only $Sc_3N@C_{68}$ was found). The main results can be summarized as follows:

(1) For the C_{78} cage, only the smallest mixed-metal nitride cluster with one Gd atom, $GdSc_2N$, can be entrapped in $GdSc_2N@C_{78}$, which was found in two different fractions, pointing to the formation of two isomers.

(2) For the C_{80}-I_h cage, the maximum yield is found for $GdSc_2N@C_{80}$. The yield of $Sc_3N@C_{80}$ is ca. 3 times lower, while that of $Gd_2ScN@C_{80}$ is ca. 4 times lower. For the C_{80}-D_{5h} cage, the distribution is shifted to the smaller cluster sizes: the yield of $Sc_3N@C_{80}$-D_{5h} is higher than that of $GdSc_2N@C_{80}$-D_{5h}. Under conditions used in this work, $Gd_3N@C_{80}$ was not detected in the Gd−Sc system.

(3) The formation of two fullerene products with one or two Gd atoms in the C_{82} carbon cage, $GdSc_2N@C_{82}$ and $Gd_2ScN@C_{82}$, is observed with a net yield of ca. 0.6%. The low stability of these fullerenes under ambient conditions did not allow their complete purification and characterization.

(4) The formation of NCFs with both $GdSc_2N$ and Gd_2ScN clusters and the absence of Sc_3N-NCFs are found for C_{84} and C_{86} cages. For these larger cage sizes, the product distribution shifts toward the structures with two Gd atoms, which are obtained in considerably higher relative yield in comparison to the NCFs with the $GdSc_2N$ cluster. In parallel, $Gd_3N@C_{84}$ is not detected at all, and $Gd_3N@C_{86}$ is formed in trace amounts (i.e., the compound was detected by mass spectrometry only). Two isomers are formed for $GdSc_2N@C_{84}$.

(5) For the C_{88} cage, the formation of $Sc_3N@C_{88}$ and $GdSc_2N@C_{88}$ is not detected at all, whereas $Gd_2ScN@C_{88}$ is the main NCF with this carbon cage. Although still small, the yield of $Gd_3N@C_{88}$ is appreciably higher than that of $Gd_3N@C_{86}$.

Spectroscopic Characterization and Structure Elucidation of $Gd_xSc_{3-x}N@C_{2n}$ NCFs: General Remarks. The molecular and electronic structures of the isolated $Gd_xSc_{3-x}N@C_{2n}$ NCFs are analyzed here based on vis−near-IR (NIR) absorption and IR spectroscopy as well as density functional theory (DFT) computations, which have been demonstrated to be powerful tools in predicting the molecular and electronic structures of fullerenes (Figure 2). The electronic absorptions of endohedral fullerenes are usually dominated by the features of the carbon cage and are mainly due to $\pi-\pi^*$ transitions of the fullerene cage rather than of the encaged species.[6,65] Thus, the optical spectra are very sensitive to the cage size and isomerism and are often used to elucidate the molecular structures of new endohedral metallofullerenes (EMFs) by comparing them with the spectra of isostructural EMFs of other metals. Because the molecular structures of major $M_3N@C_{2n}$ fullerenes are well established (at least, for major isomers) and their absorption spectra are available in the literature, these data can be used to make conclusions on the cage structures of the Gd−Sc NCFs isolated in this work. The characteristic spectral onsets and absorption data as well as the lowest limit of the optical band gaps estimated from the spectral onsets are listed in Table S2 in the SI. On the basis of these data, all presented structures can be ascribed to kinetically stable fullerenes with band gaps exceeding 1.0 eV.

Vibrational spectra also provide information on the molecular structure and cluster−cage interactions in EMFs.[66] The structures of the synthesized fullerenes can be elucidated based on a comparison of the measured spectra with the experimentally available spectra of NCFs of known structures and/or with theoretically calculated spectra. Carbon cage vibrations are very structure-sensitive and are especially suitable for this goal. Because of the substantially increased complexity and computational time required for the modeling of Gd-containing EMFs, in this work computations of vibrational spectra are performed for isostructural $Y_xSc_{3-x}N@C_{2n}$ NCFs. The ionic radius of Y^{3+} (0.90 Å) is very close to that of Gd^{3+}

dx.doi.org/10.1021/ic400049k | Inorg. Chem. 2013, 52, 3368−3380

(0.94 Å), and hence the electronic structure and vibrational spectra of Y- and Gd-based NCFs are rather similar, which was well documented in many earlier works.[18,20,64,66] The replacement of gadolinium by yttrium mostly affects low-frequency modes involving motions of metal atoms. Because of the large mass of metal atoms, these modes are not accessible in the standard IR spectra (covering wavenumbers higher than 400 cm^{-1}). The difference in the ionic radii of Gd^{3+} and Y^{3+} may also somewhat affect the metal−nitrogen bond lengths and vibrational frequencies. Finally, the cage modes can hardly be affected at all.

$Gd_xSc_{3-x}N@C_{78}$. The isomerism of NCFs with C_{78} carbon cages is an illustrative example of the nitride cluster size influence on the molecular structure. An extended computational study of C_{78} isomers in their hexaanionic state showed that two isomers of C_{78}^{6-} should be considered as possible hosts for nitride clusters.[26] The IPR-obeying isomer $D_{3h}(5)$ was found to be the most stable isomer of C_{78}^{6-}, and this isomer is proven for $Sc_3N@C_{78}$ with the planar Sc_3N cluster inside. However, for larger clusters such as Lu_3N, Y_3N, or La_3N, encapsulation inside the non-IPR isomer $C_2(22010)$ with two pairs of adjacent pentagons is much more energetically favorable. The reason for the change is the limited space inside C_{78}-$D_{3h}(5)$, which forces large clusters to be pyramidal. On the contrary, the flattened $C_2(22010)$ cage provides sufficient space for large nitride clusters to retain their planar shape. Experimental spectroscopic studies proved the $C_2(22010)$ cage isomer for $M_3N@C_{78}$ with M = Dy, Tm, and Y,[26,67] whereas the structure of $Gd_3N@C_{78}$-$C_2(22010)$ was verified by single-crystal X-ray diffraction.[68] An interesting question is how the availability of mixed $Gd_xSc_{3-x}N$ clusters of different sizes can affect the isomerism of C_{78}-based NCFs. To clarify this point, we have computed the relative energies of the $Gd_xSc_{3-x}N@C_{78}$ and $Y_xSc_{3-x}N@C_{78}$ (x = 0−3) isomers with $D_{3h}(5)$ and $C_2(22010)$ carbon cages. In agreement with the earlier studies,[26,67] the values listed in Table 2 demonstrate the preference of the $D_{3h}(5)$ isomer for $Sc_3N@C_{78}$ (73 kJ/mol below that of the C_2 isomer) and the $C_2(22010)$ isomer for $Gd_3N@C_{78}$ (116 kJ/mol below that of the D_{3h} isomer). The isomers with mixed-metal clusters exhibit intermediate relative energies. Note that $M_3N@C_{78}$-$C_2(22010)$ has two kinds of metal atoms: two of them are coordinated to adjacent pentagon pairs (APPs), and one is coordinated to the hexagon. For mixed-metal clusters, this situation leads to an additional isomerism (the barriers to the cluster rotation are expected to be high because adjacent pentagons are not stabilized by the metal in the transition state and also because of the dimensions of the cage, which favor specific positions of the cluster). Computational studies show that the isomers in which Y or Gd atoms coordinate adjacent pentagons [one for MSc_2N (Figure 3a) and two for M_2ScN clusters] are more stable than the isomers in which one or two APPs are coordinated by Sc atoms. For $Gd_2ScN@C_{78}$, DFT predicts that the $C_2(22010)$ cage is still significantly (85 kJ/mol) more preferable than $D_{3h}(5)$ (for the Y_2ScN cluster the trend is similar, but the relative energies of $D_{3h}(5)$-based isomers are smaller, in accordance with the smaller size of the Y^{3+} ion; the values computed in this work are in close agreement with the results of a recent computational study of $Y_xSc_{3-x}N@C_{78}$ by Wang et al.[67]). For the $GdSc_2N$ cluster, the energies of $C_2(22010)$ and $D_{3h}(5)$ cage isomers are almost equal, with the non-IPR-based structure being more stable by 6 kJ/mol. The $GdSc_2N$ cluster inside the C_{78}-$D_{3h}(5)$ cage is planar, but Sc−N and Gd−N bonds are much shorter

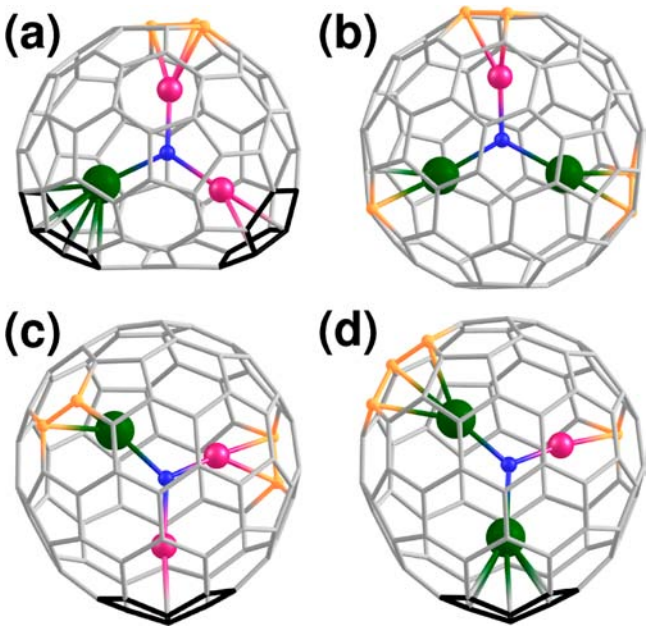

Figure 3. DFT-optimized molecular structures of the most stable conformers: (a) $GdSc_2N@C_{78}$-$C_2(22010)$; (b) $Gd_2ScN@C_{88}$-$D_2(45)$; (c) $GdSc_2N@C_{84}$-$C_s(51365)$; (d) $Gd_2ScN@C_{84}$-$C_s(51365)$. Carbon cages are shown as gray sticks (except for APPs, highlighted in black, and the atom with the smaller metal−carbon distance, shown as small yellow spheres); Gd and Sc atoms are shown as green and magenta spheres; the difference in their radii is artificially exaggerated for the sake of clarity.

than those in the $C_2(22010)$ isomer. Interestingly, substitution of gadolinium by the slightly smaller yttrium results in a change of the most favorable structure: the $YSc_2N@C_{78}$-$D_{3h}(5)$ isomer is 14 kJ/mol below the energy of $YSc_2N@C_{78}$-$C_2(22010)$. In summary, DFT computations show that the $C_2(22010)$ cage is energetically favorable for all $Gd_xSc_{3-x}N@C_{78}$ (x = 1−3) structures, starting already from one Gd atom in the cluster. At the same time, the stability of $GdSc_2N@C_{78}$-$D_{3h}(5)$ is still comparable to its non-IPR counterpart, and hence two isomers can be expected for $GdSc_2N@C_{78}$.

Analysis of the synthesized fullerene mixture showed that the main NCF with a C_{78} cage is $Sc_3N@C_{78}$-$D_{3h}(5)$. $Gd_2ScN@C_{78}$ and $Gd_3N@C_{78}$ NCFs are not detected by mass spectrometry even in trace amounts, whereas $GdSc_2N@C_{78}$ is found in fractions **1** and **5** eluting at 29.4−31.8 and 39.9−42.4 min, respectively. A substantial difference in their retention times indicates that these fractions contain two isomers of $GdSc_2N@C_{78}$ (hereafter the isomers will be denoted as I and II according to their retention times). Very tiny amounts of $GdSc_2N@C_{78}$(I) preclude its isolation and further characterization, but the fact that it elutes together with $Sc_3N@C_{78}$ indicates that presumably it has the $D_{3h}(5)$ cage. The yield of $GdSc_2N@C_{78}$(II) is significantly higher (0.6% of the total NCF yield), which provides sufficient amounts for its detailed spectroscopic characterization.

The vis−NIR spectrum of $GdSc_2N@C_{78}$(II) is compared to the spectra of $Sc_3N@C_{78}$-$D_{3h}(5)$ and $Dy_3N@C_{78}$-$C_2(22010)$ in Figure 2a. It can be clearly seen that the spectrum of $GdSc_2N@C_{78}$(II) with one weak absorption near 600 nm is similar to that of $Dy_3N@C_{78}$. The spectrum of $Sc_3N@C_{78}$-$D_{3h}(5)$ exhibits two strong absorption bands at 450 and 614 nm and is quite different from the other spectra.

dx.doi.org/10.1021/ic400049k | Inorg. Chem. 2013, 52, 3368−3380

This suggests that $GdSc_2N@C_{78}$(II) is likely to have a C_2(22010) cage symmetry.

The Fourier transform infrared (FTIR) spectrum of $GdSc_2N@C_{78}$ is shown in Figure 4 in comparison to the

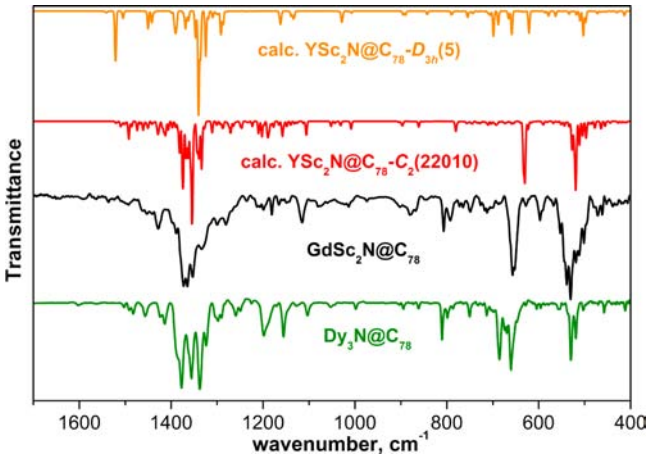

Figure 4. Experimental FTIR spectra of $GdSc_2N@C_{78}$ and $Dy_3N@C_{78}$ compared with the theoretical spectra of $YSc_2N@C_{78}$ with C_2(22010) and D_{3h}(5) cage isomers.

experimental spectrum of $Dy_3N@C_{78}$ and DFT-computed spectra of $YSc_2N@C_{78}$-C_2(22010) and $YSc_2N@C_{78}$-D_{3h}(5). In agreement with the vis−NIR spectroscopic data, the computed IR spectrum of the C_2(22010) isomers matches the experimental data much better than the spectrum of the D_{3h}(5) isomer. Thus, both spectroscopic techniques confirm that the main $GdSc_2N@C_{78}$ isomer has a C_2(22010) carbon cage with gadolinium coordinating the APP. Interestingly, the spectrum of $GdSc_2N@C_{78}$(II) is noticeably different from that of $Dy_3N@C_{78}$-C_2(22010). In particular, the different spectral patterns for a set of intense absorptions due to C−C stretching modes at 1300−1500 cm^{-1} can be pointed out. In contrast, FTIR spectra of the $Gd_xSc_{3-x}N@C_{80}$-I_h(7) family studied earlier did not vary so much with the cluster composition, and the only difference was found in the range of the cluster modes. Thus, when a less symmetric cluster and a cage are used, the change of the lanthanide to scandium results in a stronger perturbation of the cage vibrational modes.

$Gd_xSc_{3-x}N@C_{82}$. Earlier computational studies showed that three isomers of C_{82}, IPR isomer C_{2v}(9) and non-IPR isomers C_{2v}(39705) and C_s(39663), are the most suitable carbon cages for encapsulation of the nitride cluster.[62] For $Sc_3N@C_{82}$, extended DFT calculations performed in this work showed the preference of the C_{2v}(9) isomer, which is 15 kJ/mol more stable than the two non-IPR structures (see Table 2 and the SI for more details). With an increase in the cluster size, the non-IPR isomers become more energetically favorable, and the isomer C_{2v}(39705) is the most stable structure for $Gd_3N@C_{82}$, followed by C_s(39963) and C_{2v}(9) with relative energies of 26.4 and 36.5 kJ/mol. A single-crystal X-ray diffractions study of $Gd_3N@C_{82}$ proved that this NCF has a C_s(39663) carbon cage,[69] whereas the more stable isomer C_{2v}(39705) has not been observed so far. Presumably, this can be explained by kinetic reasons because C_{82}-C_{2v}(39705) is very similar to C_{80}-I_h(7).[62] Namely, removal of the C_2 unit from the pentagon/pentagon edge of the former results in C_{80}-I_h(7), and hence in the arc-discharge synthesis, $Gd_3N@C_{82}$-C_{2v}(39705) is not accumulated because of the relative ease of its rearrangement to the more stable IPR isomer $Gd_3N@C_{80}$-I_h(7).

For the intermediate-size $GdSc_2N$ and Gd_2ScN clusters, the C_{2v}(9) cage isomer is still more energetically preferable than C_s(39663), although the energy difference is decreasing with increasing cluster size. DFT shows that all $Gd_xSc_{3-x}N@C_{82}$-C_{2v}(9) structures have a low HOMO−LUMO gap and hence are not kinetically stable. Thus, the low kinetic stability of $Sc_3N@C_{82}$, $GdSc_2N@C_{82}$, and $Gd_2ScN@C_{82}$, which precluded their isolation and further spectroscopic characterization in this work, may be explained by the formation of NCFs with C_{82}-C_{2v}(9) carbon cages.

$Gd_xSc_{3-x}N@C_{84}$. Computational studies revealed that the isomers C_s(51365) and D_2(21) are the most suitable ones for the formation of $M_3N@C_{84}$ because they are almost isoenergetic in the 6− charge state.[62] For $Gd_3N@C_{84}$, DFT shows that the non-IPR C_s(51365) isomer is 41.6 kJ/ml more stable and has a noticeably higher HOMO−LUMO gap than the IPR D_2(21) isomer. C_s(51365) remains so far the only structurally characterized cage isomer of $M_3N@C_{84}$ (M = Gd,[37] Tb,[25] Tm,[37] Y[9]). Another isomer was also isolated for $Dy_3N@C_{84}$,[30] but its structural characterization is not reported yet.

For mixed-metal NCFs, DFT shows that, with a decrease in the cluster size in the $Gd_xSc_{3-x}N@C_{84}$ series, the energy difference between isomers C_s(51365) and D_2(21) is also decreasing to 31 kJ/mol for x = 2 and 17 kJ/mol for x = 1 (Table 2), and hence the two isomers can compete for NCFs with larger content of scandium. On the other hand, the HOMO−LUMO gap for D_2(21)-based $M_3N@C_{84}$ NCFs is less than 1 eV and is ca. 0.45 eV smaller than that for the NCFs with C_s(51365) cages. The low symmetry of the C_s(51365) cage provides the possibility for further isomerism for mixed-metal NCFs caused by coordination of the metal atoms to the APP: in the lowest-energy isomer of $GdSc_2N@C_{84}$-C_s(51365), the APP is coordinated by a Sc atom, whereas in the most stable $Gd_2ScN@C_{84}$-C_s(51365), the APP is coordinated by a Gd atom (Figure 3 and see the SI for further details).

Figure 2b compares vis−NIR absorption spectra of $GdSc_2N@C_{84}$(II) and $Gd_2ScN@C_{84}$ isolated in this work to the spectra of the two isomers of $Dy_3N@C_{84}$. The spectrum of $Gd_2ScN@C_{84}$ closely resembles that of $Dy_3N@C_{84}$(II) with a C_s(561365) carbon cage (as well as the spectra of other $M_3N@C_{84}$-C_s(51365) NCFs reported in the literature[19,25,36,70]). In particular, the characteristic feature at 627 nm and the absorption onset at ca. 900 nm can be pointed out. At the same time, the spectrum is drastically different from the spectrum of $Dy_3N@C_{84}$(I), whose absorptions are shifted to the NIR range. The absorption spectrum of $GdSc_2N@C_{84}$(II) exhibits more pronounced differences from the spectra of $Dy_3N@C_{84}$(II) and $Gd_2ScN@C_{84}$. First, the peak near 630 nm is split into two overlapping transitions at ca. 590 and 630 nm. Besides, new weak features at 780 and 875 nm can be seen. Nevertheless, the overall spectral pattern still resembles that of $M_3N@C_{84}$(II), suggesting that the C_s(51365) cage isomer can be assigned to $GdSc_2N@C_{84}$(II) as well. Conclusions based on the absorption spectra and DFT calculations are further corroborated by vibrational spectroscopy, which shows good agreement between the experimental FTIR spectra of $Gd_2ScN@C_{84}$ and $GdSc_2N@C_{84}$ and the DFT-computed spectra of $YSc_2N@C_{84}$ and $Y_2ScN@C_{84}$ with C_s(51365) cages (Figure 5).

dx.doi.org/10.1021/ic400049k | Inorg. Chem. 2013, 52, 3368−3380

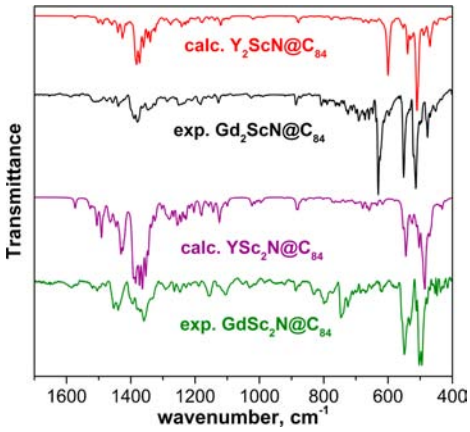

Figure 5. Experimental FTIR spectra of $GdSc_2N@C_{84}$ and $Gd_2ScN@C_{84}$ compared with the theoretical spectra of $YSc_2N@C_{84}$ and $Y_2ScN@C_{84}$ with $C_s(51365)$ cage isomers.

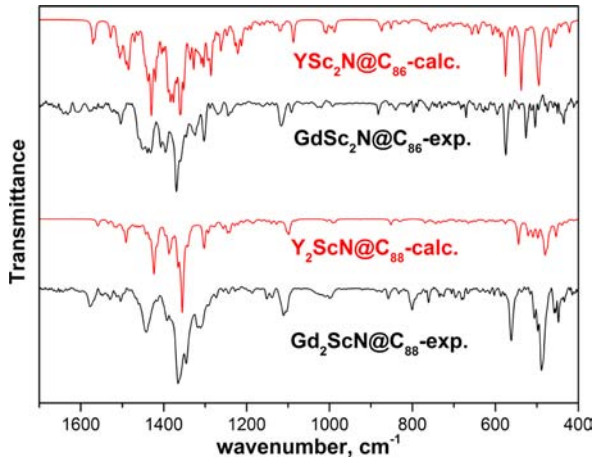

Figure 6. Experimental FTIR spectra of $GdSc_2N@C_{86}$ and $Gd_2ScN@C_{88}$ compared to the theoretical spectra of $YSc_2N@C_{86}$-$D_3(17)$ and $Y_2ScN@C_{88}$-$D_2(35)$.

On the basis of the results of DFT studies (Table 2), the yet nonisolable isomer $GdSc_2N@C_{84}(I)$ eluting in fraction **5** at 40−43 min can be preliminary assigned to the $D_2(21)$ cage; however, an unambiguous structural assignment should be deferred until further separation and spectroscopic studies are done.

$Gd_xSc_{3-x}N@C_{86}$. Only one isomer of $M_3N@C_{86}$ has been synthesized and isolated so far for several lanthanides and yttrium,[9,22,30,36] and its cage structure determined by single-crystal X-ray diffraction is $D_3(17)$.[21,24] Likewise, DFT studies favor the $D_3(17)$ isomer as the lowest-energy hexaanion of C_{86}, which has a sufficiently high HOMO−LUMO gap.[62] Although isomers $C_{2v}(7)$ and $C_s(13)$ also provide thermodynamically stable $M_3N@C_{86}$ structures,[62] their small HOMO−LUMO gaps (~0.6 eV) make the formation of stable NCFs with these cages unlikely. Results of this work also show that only one cage isomer is formed for $GdSc_2N@C_{86}$ and $Gd_2ScN@C_{86}$ in appreciable amounts.

Figure 2c compares the absorption spectra of $GdSc_2N@C_{86}$ and $Gd_2ScN@C_{86}$ isolated in this work to the spectra of $Dy_3N@C_{86}$[30] and $Tm_3N@C_{86}$.[36] Even for monometal $M_3N@C_{86}$ NCFs, the spectral pattern shows a noticeable metal dependence, as can be concluded from the shift of the strong absorption band seen at 640 nm in the spectrum of $Dy_3N@C_{86}$ to ca. 600 nm in the spectrum of $Tm_3N@C_{86}$; the spectra of $Tb_3N@C_{86}$ and $Gd_3N@C_{86}$ reported in refs 24 and 70 are similar to that of $Dy_3N@C_{86}$. The spectral pattern of $Gd_2ScN@C_{86}$ follows the spectra of other $M_3N@C_{86}$ NCFs but shows features already discussed for other Gd−Sc mixed NCFs. Namely, absorption bands in the spectrum of the mixed-metal NCF are broadened and split (e.g., the band at 640 nm is split into two overlapping bands at 596 and 725 nm). In contrast, $GdSc_2N@C_{86}$ exhibits a featureless spectrum with the onset at ca. 1000 nm, and hence the absorption spectrum of $GdSc_2N@C_{86}$ does not allow its structural assignment. However, the compound does exhibit a well-resolved IR spectrum (Figure 6), which agrees well with the computed spectrum of $YSc_2N@C_{86}$-$D_3(17)$.

$Gd_2ScN@C_{88}$. According to experimental[24,30,42,71] and computational[62,72] studies, the only plausible cage isomer of $M_3N@C_{88}$ (M = Y, Gd−Lu) is $D_2(35)$. When both scandium and gadolinium are available in the arc-discharge synthesis, the only C_{88}-based NCF obtained in isolable amounts is $Gd_2ScN@C_{88}$, whereas the yield of $Gd_3N@C_{88}$ (which is one of the main products in the Gd_3N NCFs synthesis) is an order of magnitude lower (Table 1). The absorption spectrum of $Gd_2ScN@C_{88}$ isolated in this work exhibits a pronounced similarity to the spectrum of $Dy_3N@C_{88}$ (Figure 2d) and allows the assignment of the cage structure of $Gd_2ScN@C_{88}$ to $D_2(35)$ as well. In particular, quite characteristic is the absorption band at 1073 nm, which is also observed in other $M_3N@C_{88}$-$D_2(35)$ NCFs near this wavelength (e.g., at 1063 nm in $Dy_3N@C_{88}$). Another characteristic absorption of $M_3N@C_{88}$-$D_2(35)$ NCFs at 730−750 nm (e.g., 733 nm in $Dy_3N@C_{88}$) is split into two bands at 670 and 740 nm in the spectrum of $Gd_2ScN@C_{88}$. The very good match of the experimental IR spectrum of $Gd_2ScN@C_{88}$ with the DFT-computed spectrum of $Y_2ScN@C_{88}$-$D_2(35)$ (Figure 6) serves as an additional confirmation of the $D_2(35)$ cage structure of the isolated $Gd_2ScN@C_{88}$.

Effect of Scandium on the Electronic and Molecular Structures of $Gd_xSc_{3-x}N@C_{2n}$. The similarity of the spectra of EMFs with the same carbon cage sizes in the same charge state and with different metals and clusters holds only if the metal atoms do not contribute to the frontier orbitals and/or the metal-based excitations have low intensities. Spectroscopic studies of the Gd−Sc mixed NCFs described in the previous sections show that substitution of gadolinium with scandium in $M_3N@C_{2n}$ compounds with the same carbon cage imposes a profound effect on the absorption spectra of the NCFs. The subtle effect of the scandium-to-gadolinium substitution was already pointed out earlier for $Gd_xSc_{3-x}N@C_{80}$,[18,20] and the results of this work evidence that this effect is of a general nature and can be more enhanced for other carbon cages. Absorption features in the spectra of Sc-containing NCFs are sometimes split and usually broader than those in the non-Sc-containing NCFs with the same carbon cage. Besides, the absorption onset has a tendency to shift to the NIR range. In the series of compounds studied in this work, the effect of scandium is most pronounced for $Gd_xSc_{3-x}N@C_{86}$. While the spectrum of $Gd_2ScN@C_{86}$ is still similar to $M_3N@C_{86}$, the features in the spectrum of $GdSc_2N@C_{86}$ are so broadened that they can hardly be distinguished. Because the absorption spectra of NCFs with other lanthanides are rather similar, variation of the absorption spectra of Sc−Gd NCFs can be ascribed to the special role of scandium.

dx.doi.org/10.1021/ic400049k | Inorg. Chem. 2013, 52, 3368−3380

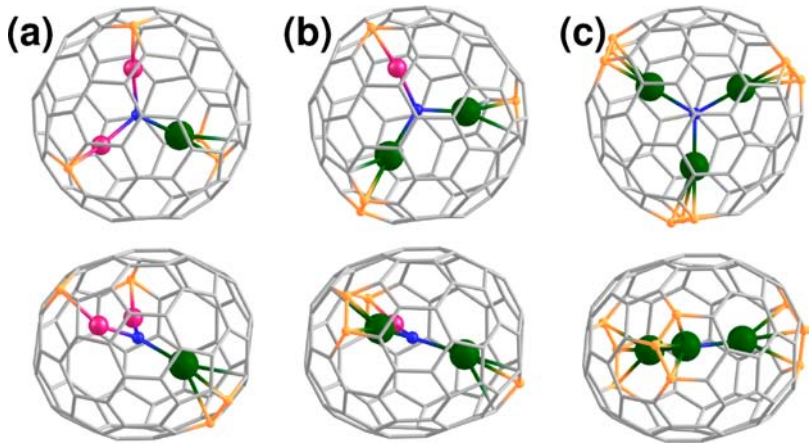

Figure 7. DFT-optimized molecular structures of the lowest-energy conformers of (a) $GdSc_2N@C_{86}$, (b) $Gd_2ScN@C_{86}$, and (c) $Gd_3N@C_{86}$. Each molecule is shown in two projections: in the upper row, a 3-fold symmetry axis of the D_3-symmetric carbon cage is perpendicular to the paper; in the bottom row, the axis is in the plane of the paper and a C_2 axis is perpendicular to it. Orientation of the carbon cages are the same in all series, so all visual differences are due to the rearrangement of the cluster.

Detailed analysis shows that scandium has a 2-fold effect on the electronic structure of $Gd_xSc_{3-x}N@C_{2n}$ molecules. First, scandium is different from yttrium and lanthanides in that it has considerably higher electronegativity and, hence, lower energies of corresponding molecular orbitals (MOs). This can result in a substantial variation of the nature of the frontier MOs for NCFs with the same carbon cage but different cluster composition. For instance, the LUMO of $Sc_3N@C_{80}$ is largely localized on the Sc_3N cluster, while the LUMO of $M_3N@C_{80}$ NCFs with other metals is to a large extent a cage orbital.[64,73] DFT-computed MO levels and isosurfaces for $Gd_xSc_{3-x}N@C_{2n}$ molecules (analyzed in the SI) show that the Sc contributions to the frontier MOs, especially LUMOs, are noticeably higher than those of Gd atoms (and, hence, the carbon cage contributions to the LUMOs are smaller than those in $Gd_3N@C_{2n}$ molecules). As a result, the HOMO−LUMO gap of $Gd_xSc_{3-x}N@C_{2n}$ molecules tends to decrease with an increase in the number of Sc atoms in the cluster, as can be inferred from the data listed in Table 2. Thus, it can be concluded that changes in the absorption spectra of the $Gd_xSc_{3-x}N@C_{2n}$ NCFs are caused by the admixing of the scandium atomic orbitals with the low-energy LUMOs of the carbon cage.

In addition to the pure electronic factor outlined above, substitution of gadolinium by scandium also has geometric consequences for the molecular structures of NCFs. The smaller ionic radius of scandium results in changes in the Gd−N and Sc−N bonds with an increase in the number of Sc atoms in the nitride cluster. This point will be discussed in the next section within the discussion of the M−N stretching modes. Besides, a decrease in the size of the whole $Gd_xSc_{3-x}N$ cluster can result in reorientation of the cluster inside the carbon cage. This phenomenon is most pronounced in the $Gd_xSc_{3-x}N@C_{86}$ series and is probably responsible for the strong variations in their absorption spectra. In $Gd_3N@C_{86}$-D_3(17), the symmetric Gd_3N cluster matches the 3-fold symmetry of the cage, and the cluster plane is located perpendicular to the C_3 axis so that the cluster adopts the largest possible space inside the somewhat flattened carbon cage (Figure 7). However, substitution of one Gd atom by a Sc atom stabilizes a different position of the Gd_2ScN fragment: the cluster is rotated around the C_3 axis of the carbon cage, and its plane is tilted with respect to the parallel arrangement of the Gd_3N cluster in $Gd_3N@C_{86}$ (Figure 7). DFT shows that the conformer of $Gd_2ScN@C_{86}$ retaining the cluster position as in $Gd_3N@C_{86}$ is 15.6 kJ/mol higher in energy. This effect is further enhanced in $GdSc_2N@C_{86}$, whose conformer with the tilted position of the $GdSc_2N$ cluster is 26.6 kJ/mol more stable than the conformer with the parallel arrangement (i.e., retaining the position of the cluster as in $Gd_3N@C_{86}$). The reason for these rearrangements is the reduced size of the Gd_2ScN cluster and especially of the $GdSc_2N$ cluster, which cannot efficiently bond the carbon cage in the parallel arrangement.

The structural variations in the $Gd_xSc_{3-x}N@C_{86}$ series (x = 1−3) are also reflected in the electronic structure of these species. Figure 8 shows their MO levels and isosurfaces of the HOMO and LUMO. Although the HOMOs of $GdSc_2N@C_{86}$, $Gd_2ScN@C_{86}$, and $Gd_3N@C_{86}$ are localized on the carbon cage and have similar spatial patterns, the changes in their shapes are clearly visible (compared to, e.g., $Gd_xSc_{3-x}N@C_{84}$ NCFs, which have almost identical HOMOs in the whole series irrespective of the cluster composition; see the SI). These changes can be ascribed to the different orientations of the cluster because the scandium contributions to HOMO are small. LUMO shapes are affected much more strongly both in terms of the increased scandium contributions to the MOs and in the changes of the MO distribution over the carbon cage. These changes result in a noticeable variation of the HOMO−LUMO gaps and the overall MO levels in $Gd_xSc_{3-x}N@C_{86}$ NCFs. Thus, it is not surprising that their absorption spectra are different.

The computations for the conformers with the parallel arrangement of the nitride cluster show that in $GdSc_2N@C_{86}$ scandium has even a more pronounced effect than in the conformer with tilted arrangement. The LUMO of $GdSc_2N@C_{86}$ is purely a Sc-based MO and is strongly stabilized, resulting in a much smaller HOMO−LUMO gap of the molecule (Figure 8a). It should be noted that at room temperature the cluster rotates, and the measured absorption spectra are superpositions of the spectra of different conformers. The larger variation of the electronic structure of $GdSc_2N@C_{86}$ with the cluster orientation obviously leads to the more pronounced effect in the spectra.

Interestingly, the changes in the cluster composition also result in strong variation of the chromatographic behavior of

dx.doi.org/10.1021/ic400049k | Inorg. Chem. 2013, 52, 3368−3380

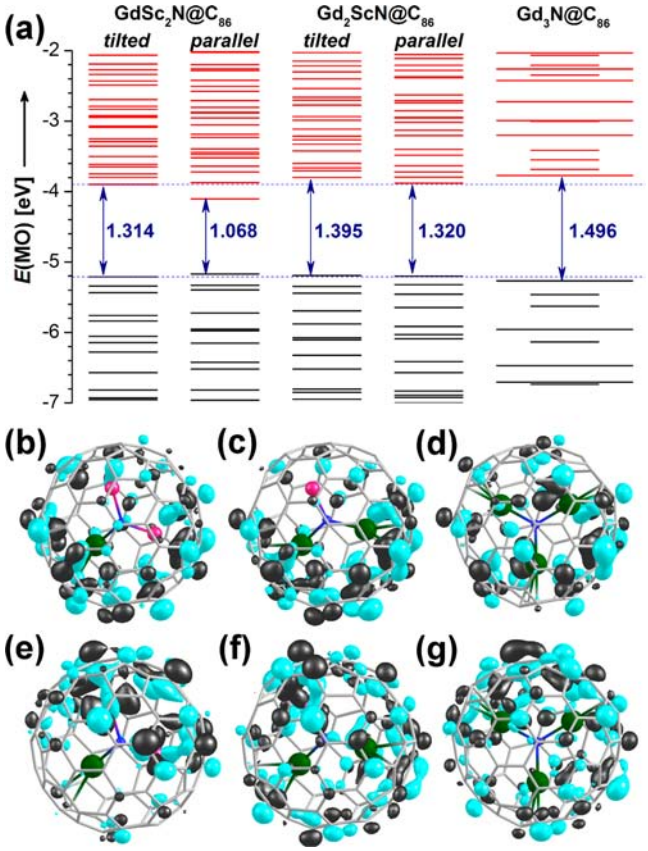

Figure 8. (a) MO energy levels in $GdSc_2N@C_{86}$, $Gd_2ScN@C_{86}$, and $Gd_3N@C_{86}$ (black, occupied orbitals; red, unoccupied orbitals); for the Gd−Sc NCFs, the levels are shown for two conformers with tilted and parallel arrangement of the nitride cluster. HOMO−LUMO gaps are indicated by two-headed arrows. HOMOs of $GdSc_2N@C_{86}$ (b), $Gd_2ScN@C_{86}$ (c), and $Gd_3N@C_{86}$ (d). LUMOs of $GdSc_2N@C_{86}$ (e), $Gd_2ScN@C_{86}$ (f), and $Gd_3N@C_{86}$ (g). MOs of $GdSc_2N@C_{86}$ and $Gd_2ScN@C_{86}$ are shown for the lowest-energy conformers with tilted arrangement of the cluster.

Gd−Sc NCFs. A comparison of the retention times of $Gd_xSc_{3-x}N@C_{2n}$ compounds (Table 3) shows that an increase

Table 3. Chromatographic Retention Times of $Gd_xSc_{3-x}N@C_{2n}$[a]

	cluster		
cage	$GdSc_2N$	Gd_2ScN	Gd_3N
C_{80}-I_h	29.4−31.8 (1)	29.4−31.8 (1)	31.4
C_{84}-C_s(51365)	51.2−53.5 (8)	45.2−46.9 (6)	41.0
C_{86}-D_3(17)	55.6−58.1 (9)	51.2−53.5 (8)	38.4
C_{88}-D_2(45)		48.8−50.9 (7)	44.9

[a]The values are determined for the linear combination of two Buckyprep columns and can vary within ca. 1 min from measurement to measurement and even more so depending on the conditions (flow rate, etc.); the numbers in parentheses indicate the number of the fraction shown in Figure 1.

in the number of Sc atoms in the cluster lengthens systematically and considerably the retention time of the NCF with larger cages. The effect is especially strong for the $Gd_xSc_{3-x}N@C_{86}$ series and is consistent with the strongest variation of the molecular and electronic structures within this group discussed above. At the same time, $GdSc_2N@C_{80}$, $Gd_2ScN@C_{80}$, and $Gd_3N@C_{80}$ with $I_h(7)$ carbon cages show almost no difference in their retention times.

Electrochemistry of $Gd_xSc_{3-x}N@C_{2n}$. In spite of the extended electrochemical studies of NCFs in the past decade, data on the mixed-metal NCFs are rather scarce. To our knowledge, there are only two reports on the redox potentials of Sc-based mixed-metal NCFs.[10,74] Wang and co-workers reported redox potentials of $Y_xSc_{3-x}N@C_{80}$-I_h and showed that the first reduction potential is shifting to positive directions with an increase in the number of Sc atoms in the cluster.[10]

Figure 9 shows cyclic voltammograms of selected $Gd_xSc_{3-x}N@C_{2n}$ NCFs, whereas Table 4 lists their redox

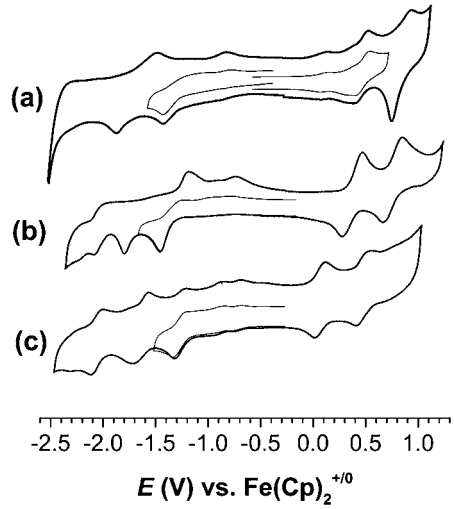

Figure 9. Cyclic voltammetry of (a) $GdSc_2N@C_{78}$, (b) $Gd_2ScN@C_{84}$, and (c) $Gd_2ScN@C_{88}$. The measurements are performed at room temperature in *o*-dichlorobenzene with 0.1 M $TBABF_4$ as the electrolyte. Scan rate = 100 mV/s.

potentials. Except for $Gd_2ScN@C_{88}$, all other compounds exhibit electrochemically irreversible reduction and reversible oxidation steps. Reductions of $Gd_2ScN@C_{88}$ appeared as more reversible processes, allowing determination of the $E_{1/2}$ potentials, although additional reoxidation peaks can be seen for this compound as well. In general, the electrochemical behavior of $Gd_xSc_{3-x}N@C_{2n}$ NCFs, including the reversible reductions of $Gd_2ScN@C_{88}$, is similar to that of the corresponding $Gd_3N@C_{2n}$ NCFs reported by Echegoyen et al.[19,68]

A comparison of the redox potentials of $Gd_3N@C_{78}$ and $Gd_3N@C_{88}$ shows that the oxidation potentials of mixed-metal NCFs are close to those of Gd_3N-NCFs (within the uncertainty of measurements of 0.01−0.02 V), whereas the reduction potentials are shifted positively, resulting thus in smaller electrochemical gaps. The positive shift of the reduction potentials in the Gd−Sc NCFs agrees with the DFT-predicted stabilization of the LUMO due to an increase of the scandium contribution. Likewise, the changes in the electrochemical gaps correlate with a decrease in the DFT-computed HOMO−LUMO gaps (Table 2).

For $Gd_2ScN@C_{84}$, the situation in redox reactions is different because its oxidation is found at more positive potentials than that reported for $Gd_3N@C_{84}$, whereas the first reduction occurs at more negative potentials. The electrochemical gap is thus larger in $Gd_2ScN@C_{84}$ than in $Gd_3N@C_{84}$ (Table 4). This finding also agrees with the results of DFT computations

dx.doi.org/10.1021/ic400049k | Inorg. Chem. 2013, 52, 3368−3380

Table 4. Redox Potentials of $Gd_xSc_{3-x}N@C_{2n}$ [a]

NCF	method[b]	II_{ox}	I_{ox}	I_{red}	II_{red}	III_{red}	gap_{EC}
$GdSc_2N@C_{78}$	CV	[0.92]	0.45	[−1.44]	[−1.88]		1.89
	SWV	0.84	0.46	−1.38	−1.86		1.84
$Gd_3N@C_{78}$[c]	CV	[1.00]	0.47	[−1.53]	[−1.89]		2.00
$GdSc_2N@C_{80}$	CV		0.64	[−1.32]			1.96
	SWV	1.11	0.66	−1.27	−1.88	−2.29	1.93
$Gd_2ScN@C_{80}$	CV		0.66	[−1.36]			2.02
	SWV	1.06	0.67	−1.33	−1.78		1.99
$Gd_3N@C_{80}$[d]	CV		0.58	[−1.44]	[−1.86]	[−2.15]	2.02
$Gd_2ScN@C_{84}$	CV	0.74	0.37	[−1.44]	[−1.80]	[−2.08]	1.81
	SWV	0.76	0.37	−1.39	−1.78		1.76
$Gd_3N@C_{84}$[d]	CV		0.32	[−1.37]	[−1.76]		1.69
$Gd_2ScN@C_{88}$	CV	0.48	0.07	−1.26	−1.63	−2.05	1.33
	SWV	0.49	0.08	−1.26	−1.63	−2.05	1.34
$Gd_3N@C_{88}$[d]	CV	0.49	0.06	−1.38	−1.69		1.44

[a]Potentials are measured versus the $Fe(Cp)_2^{+/0}$ couple; peak potentials for the electrochemically irreversible steps are given in square brackets. [b]CV = cyclic voltammetry; SWV = square-wave voltammetry; [c]From ref 68. [d]From ref 19.

Table 5. Antisymmetric Metal−Nitrogen Stretching Modes in Selected $Gd_xSc_{3-x}N@C_{2n}$ Molecules and Their Assignment Based on PED Analysis

NCF	ν_{exp}, cm^{-1}	ν_{calc}[a] cm^{-1}	PED, %
$GdSc_2N@C_{78}$	531 (br)	518−527	36% Sc2−N + 25% Gd−N
	655	630/633	52% Sc1−N
$GdSc_2N@C_{80}$[b]	647	622	37% Gd−N + 32% Sc−N
	694	658	48% Sc−N
$Gd_2ScN@C_{80}$[b]	649, 656	658	55% Gd−N
	759	718−729	49% Sc−N
$GdSc_2N@C_{84}$	495/503	485/489/495	32% Sc2−N + 16% Gd−N
	548	544	41% Sc1−N + 18% Gd−N
$Gd_2ScN@C_{84}$	512	508	8% Gd−N
	550	538	29% Gd2−N + 14% Gd1−N
	628	600	34% Sc−N + 13% Gd1−N
$GdSc_2N@C_{86}$	526	537	58% Sc−N
	575	575	37% Sc−N + 26% Gd−N
$Gd_2ScN@C_{88}$	485/490	474−487	49% Gd−N + 12% Sc−N
	562	543	43% Sc−N + 10% Gd−N

[a]Frequencies are calculated for $Y_xSc_{3-x}N@C_{2n}$ molecules. [b]From ref 20.

showing an increase in the HOMO−LUMO gap in $Gd_2ScN@C_{84}$ in comparison to $Gd_3N@C_{84}$ (Table 2).

Cluster Vibrations and Metal−Nitrogen Bond Lengths. The information on the internal structure of the nitride cluster can be obtained from the vibrational spectra of NCFs. In particular, the antisymmetric metal−nitrogen stretching mode visible in the IR spectra near 500−750 cm^{-1} correlates well with the metal−nitrogen bond lengths and the shape of the cluster.[66] In a symmetric M_3N cluster, this mode is 2-fold-degenerate, whereas in the mixed-metal M_2LN cluster, it is split into two components, whose frequencies are proportional to $(3k_{M-N})^{1/2}$ and $(2k_{L-N} + k_{M-N})^{1/2}$ according to a phenomenological analysis (here k_{M-N} and k_{L-N} are metal−nitrogen force constants).[66] Thus, the two vibrations can be denoted as ν_{M-N} and ν_{L-N} and associated with vibrations of the corresponding metal−nitrogen bonds (although for ν_{L-N}, it is not completely correct because of the admixture of the metal−nitrogen vibration). The numerous studies of mixed-metal $M_xSc_{3-x}N@C_{80}$ NCFs[3,10,18,20,33,40,75] (M = Y and lanthanides) revealed that the ν_{M-N} frequency is decreasing in the M_3N−M_2ScN−MSc_2N row, whereas ν_{Sc-N} is increasing in the Sc_3N−MSc_2N−M_2ScN row because the metal−nitrogen bonds are elongated to release the internal strain with an increase in the number of Sc atoms in the cluster, and Sc−N bond lengths are shorter in the mixed-metal cluster than in Sc_3N. For instance, ν_{Sc-N} modes in $Sc_3N@C_{80}$, $GdSc_2N@C_{80}$, and $Gd_2ScN@C_{80}$ are found at 599, 654, and 759 cm^{-1}, respectively.[20] For the $Gd_xSc_{3-x}N@C_{2n}$ molecules studied in this work, phenomenological analysis appeared to be oversimplified because of the large asymmetry of the cluster. Hence, we interpreted the metal−nitrogen stretching vibrations using potential energy distribution (PED) analysis. Table 5 lists the experimental and computed frequencies as well as their interpretation in terms of PED. Table 6 lists the DFT-optimized metal−nitrogen bond lengths in $Gd_xSc_{3-x}N@C_{2n}$.

In the spectrum of $GdSc_2N@C_{78}$, the strong absorption at 655 cm^{-1} is assigned to the stretching mode of the Sc1−N bond involving the Sc atom coordinated to a hexagon. According to DFT calculations, the length of this bond is 1.963 Å. The Sc2−N bond with an APP-coordinated Sc atom is much longer (2.027 Å), and its vibration mixed with the vibration of the Gd−N bond and the cage modes appears as a group of medium-to-strong bands around 531 cm^{-1}. In $GdSc_2N@C_{80}$, the ν_{Sc-N} mode at 694 cm^{-1} has the highest

dx.doi.org/10.1021/ic400049k | Inorg. Chem. 2013, 52, 3368−3380

Table 6. DFT-Optimized Gd−N and Sc−N Bond Lengths (Å) in Selected $Gd_xSc_{3-x}N@C_{2n}$ Molecules

	cluster		
cage	$GdSc_2N$	Gd_2ScN	Gd_3N
C_{78}-C_2(22010)	Gd: 2.254	Gd1: 2.113	Gd1: 2.066
	Sc1: 1.963	Gd2: 2.184[b]	Gd2,Gd3: 2.104[b]
	Sc2: 2.027*	Sc: 1.968	
C_{80}-I_h(7)[a]	Gd: 2.168	Gd1: 2.105	2.080
	Sc1: 1.964	Gd2: 2.110	
	Sc2: 1.968	Sc: 1.910	
C_{84}-C_s(51365)	Gd: 2.260	Gd1: 2.193	Gd1: 2.133
	Sc1: 2.028	Gd2: 2.237[b]	Gd2: 2.133
	Sc2: 2.081[b]	Sc: 1.979	Gd3: 2.170[b]
C_{86}-D_3(17)	Gd: 2.262	Gd1: 2.191	2.162
	Sc1: 2.019	Gd2: 2.207	
	Sc2: 2.033	Sc: 1.977	
C_{88}-D_2(45)	Gd: 2.377	Gd1: 2.262	Gd1, Gd2: 2.185
	Sc1: 2.039	Gd2: 2.263	Gd3: 2.186
	Sc2: 2.088	Sc: 1.997	

[a]From ref 20. [b]Metal atom, coordinated to the APP.

frequency among all structures with the $GdSc_2N$ cluster, whereas the mode with mixed Gd−N/Sc−N character is found at 647 cm^{-1}. The softest ν_{M-N} modes of the $GdSc_2N$ cluster are found in $GdSc_2N@C_{84}$ and are assigned to the bands near 500 cm^{-1} and at 548 cm^{-1}. The former is due to the stretching vibration of the longer Sc2−N bond (2.081 Å; Sc2 is coordinating the pentagon pair), whereas the higher-frequency band is due to the shorter Sc1−N bond. The stretching vibration of the Gd−N bond in $GdSc_2N@C_{84}$ is contributing equally to both modes. The frequencies of the metal−nitrogen vibrations in $GdSc_2N@C_{86}$ are significantly higher than those in $GdSc_2N@C_{84}$ but are much softer than those in $GdSc_2N@C_{78}$ and $GdSc_2N@C_{80}$. The lower-frequency mode at 526 cm^{-1} is a pure Sc−N vibration (two Sc−N bonds are similar, 2.019 and 2.033 Å, and hence contributing equally), while significant contributions of the Gd−N bond is found only for the higher-frequency component at 575 cm^{-1}. Note that the Gd−N stretching vibrations of the smaller cage have higher contributions for the lower-frequency component.

Vibrations of the Gd_2ScN cluster undergo an expectable transformation with an increase in the cage size: a strong softening is observed from C_{80} to C_{84} to C_{88}. Both Gd−N and Sc−N dominating vibrations shift from C_{80} to C_{88} by ca. 180 cm^{-1}, in line with the considerable lengthening of the metal−nitrogen bonds (Table 6). For example, the short Sc−N bond in $Gd_2ScN@C_{80}$ (1.910 Å) is elongated to 1.997 Å in $Gd_2ScN@C_{88}$, and the ν_{Sc-N} frequency drops from ca. 720 to 543 cm^{-1}.

In summary, encapsulation of the $GdSc_2N$ and Gd_2ScN cluster in the carbon cages of different sizes and shapes results in considerable variation of the metal−nitrogen stretching vibrations, which can then be correlated to the changes in the metal−nitrogen bond lengths. With an increase of the cage size, the frequencies tend to shift to lower energies because larger cages allow longer metal−nitrogen bonds.

CONCLUSIONS

The mutual influence of the cluster and cage size on the preferable fullerene structure was studied, and a gradual decrease of the number of Sc atoms for the larger cages was observed. For this purpose, Gd-containing NCFs $Gd_xSc_{3-x}N@C_{2n}$ ($2n$ = 78−88) were synthesized using melamine as a solid source of nitrogen. It is shown that Gd_3N-NCFs were not preferable products in cages up to C_{88}. For $GdSc_2N@C_{78}$, both the D_{3h}(5) and C_2(22010) cage isomers are obtained, with the latter being the dominant structure, showing that even one Gd atom in the nitride cluster already switches the preferable cage isomer. For C_{84} and C_{86} cage sizes, both $GdSc_2N$ and Gd_2ScN cluster fullerenes are obtained, whereas for C_{88}, encapsulation of the $GdSc_2N$ cluster was not detected at all.

Substitution of gadoliniun by scandium imposes a noticeable influence on the electronic structure of NCFs, as revealed by electrochemical, spectroscopic, and computational methods. Especially the LUMO energy and the shape are affected, having a higher metal contribution and lower energy with an increase in the number of Sc atoms in the cluster. For C_{86}, the difference in the ionic radii of the metals results also in the rearrangement of the cluster inside the cage and, hence, in an even larger change of the frontier MOs.

EXPERIMENTAL SECTION

Mixed-metal cluster fullerenes were produced by evaporating graphite rods in the electric arc by the Krätschmer−Huffman method modified in our group. The graphite rods (length 100 mm; diameter 8 mm) were packed with a Gd:Sc:C:N mixture in a molar ratio of 1:1:15:10 (this ratio was found to be optimal for the best endohedral fullerene yield) and evaporated in a 200 mbar helium atmosphere with a current of 100 A. The soot produced by arc vaporization was first placed in an envelope made of filter paper and Soxhlet-extracted with acetone for 1 h to remove non-fullerene products. The soot was then dried for 1 h in a vacuum at 350 K and then Soxhlet-extracted for 20 h with carbon disulfide. Isolation of mixed-metal NCFs was first accomplished by HPLC using a combination of two analytical 4.6 mm × 250 mm Buckyprep columns (Nacalai Tesque, Japan) and toluene as the solvent. Further purification of the fractions was performed by recycling HPLC on BuckyPrep, BuckyPrep-M, and 5PYE columns (see the SI). The compositions of the fractions were analyzed by a MALDI-TOF mass spectrometer (Biflex III, Bruker, Germany).

UV−vis−NIR absorption spectra were measured at room temperature in toluene solutions on a Shimadzu 3100 spectrophotometer. For IR measurements, the sample was drop-coated onto single-crystal KBr disks. The residual toluene was removed by heating the polycrystalline films in vacuum at 200 °C for 3 h. The FTIR spectra were recorded at room temperature in transmission mode by a Vertex 80v spectrometer (Bruker, Germany) with a resolution of 2 cm^{-1}. Voltammetric experiments were performed with a PAR 273 potentiostat (EG&G, U.S.) at room temperature in a glovebox. A three-electrode system using platinum working and counter electrodes and a silver wire quasi-reference electrode was used. Potentials were measured by adding ferrocene as an internal standard.

DFT computations were performed using Priroda code[76,77] and the PBE functional.[78] For computations of the $Gd_xSc_{3-x}N@C_{2n}$ structures, the relativistic variant of the full-electron Λ1 basis ({3,2,1}/(10s,7p,3d) for C and N atoms, {6,5,3,1}/(21s,16p,11d,5f) for Sc atoms, and {9,8,6,3,1}/(30s,29p,20d,14f,6g) for Gd atoms) was used along with Dyal's version of the scalar-relativistic (SR) corrections;[79,80] the highest spin multiplicities were used for each cluster (8 for $GdSc_2N$, 15 for Gd_2ScN, and 22 for Gd_3N). The SR-PBE/Λ1 relative energies as well as MO energies are discussed throughout the text and listed in Table 2. Note that the MO energies are analyzed for the spin-up states (the spin-down energies are not correct because PBE predicts too low energies for the unoccupied Gd-based MOs). Vibrational computations were performed for $Y_xSc_{3-x}N@C_{2n}$ structures using the nonrelativistic PBE/TZ2P method with a SBK-type core potential for yttrium, as reported in the previous works.[20,26]

dx.doi.org/10.1021/ic400049k | Inorg. Chem. 2013, 52, 3368−3380

■ ASSOCIATED CONTENT

Supporting Information

Details of chromatographic separation and quantum-chemical computations, mass spectra, and Cartesian coordinates. This material is available free of charge via the Internet at http://pubs.acs.org.

■ AUTHOR INFORMATION

Corresponding Author

*E-mail: a.popov@ifw-dresden.de (A.A.P.), L.Dunsch@ifw-dresden.de (L.D.).

Notes

The authors declare no competing financial interest.

■ ACKNOWLEDGMENTS

The authors are thankful to Sandra Schiemenz (IFW Dresden) for help with spectroscopic measurements and to Ulrike Nitzsche for assistance with local computational resources in IFW Dresden. The Research Computing Center of Moscow State University and Jülich Supercomputing Center are acknowledged for time on supercomputers "SKIF-Chebyshev" and JUROPA, respectively. A.A.P. is thankful to the DFG (Project PO 1602/1-1) for financial support.

■ REFERENCES

(1) Heath, J. R.; O'Brien, S. C.; Zhang, Q.; Liu, Y.; Curl, R. F.; Tittel, F. K.; Smalley, R. E. *J. Am. Chem. Soc.* **1985**, *107* (25), 7779−7780.

(2) Stevenson, S.; Rice, G.; Glass, T.; Harich, K.; Cromer, F.; Jordan, M. R.; Craft, J.; Hadju, E.; Bible, R.; Olmstead, M. M.; Maitra, K.; Fisher, A. J.; Balch, A. L.; Dorn, H. C. *Nature* **1999**, *401* (6748), 55−57.

(3) Dunsch, L.; Krause, M.; Noack, J.; Georgi, P. *J. Phys. Chem. Solids* **2004**, *65* (2−3), 309−315.

(4) Dunsch, L.; Georgi, P.; Krause, M.; Wang, C. R. *Synth. Met.* **2003**, *135* (1−3), 761−762.

(5) Yang, S.; Zhang, L.; Zhang, W.; Dunsch, L. *Chem.—Eur. J.* **2010**, *16* (41), 12398−12405.

(6) Dunsch, L.; Yang, S. *Small* **2007**, *3* (8), 1298−1320.

(7) Chaur, M. N.; Melin, F.; Ortiz, A. L.; Echegoyen, L. *Angew. Chem., Int. Ed.* **2009**, *48*, 7514−7538.

(8) Krause, M.; Kuzmany, H.; Georgi, P.; Dunsch, L.; Vietze, K.; Seifert, G. *J. Chem. Phys.* **2001**, *115* (14), 6596−6605.

(9) Fu, W.; Xu, L.; Azurmendi, H.; Ge, J.; Fuhrer, T.; Zuo, T.; Reid, J.; Shu, C.; Harich, K.; Dorn, H. C. *J. Am. Chem. Soc.* **2009**, *131* (33), 11762−11769.

(10) Chen, N.; Fan, L. Z.; Tan, K.; Wu, Y. Q.; Shu, C. Y.; Lu, X.; Wang, C. R. *J. Phys. Chem. C* **2007**, *111* (32), 11823−11828.

(11) Chaur, M. N.; Melin, F.; Ashby, J.; Kumbhar, A.; Rao, A. M.; Echegoyen, L. *Chem.—Eur. J.* **2008**, *14* (27), 8213−8219.

(12) Wang, X. L.; Zuo, T. M.; Olmstead, M. M.; Duchamp, J. C.; Glass, T. E.; Cromer, F.; Balch, A. L.; Dorn, H. C. *J. Am. Chem. Soc.* **2006**, *128* (27), 8884−8889.

(13) Chaur, M. N.; Melin, F.; Elliott, B.; Kumbhar, A.; Athans, A. J.; Echegoyen, L. *Chem.—Eur. J.* **2008**, *14* (15), 4594−4599.

(14) Zhang, L.; Popov, A. A.; Yang, S.; Klod, S.; Rapta, P.; Dunsch, L. *Phys. Chem. Chem. Phys.* **2010**, *12*, 7840−7847.

(15) Melin, F.; Chaur, M. N.; Engmann, S.; Elliott, B.; Kumbhar, A.; Athans, A. J.; Echegoyen, L. *Angew. Chem., Int. Ed.* **2007**, *46* (47), 9032−9035.

(16) Stevenson, S.; Phillips, J. P.; Reid, J. E.; Olmstead, M. M.; Rath, S. P.; Balch, A. L. *Chem. Commun.* **2004**, *24*, 2814−2815.

(17) Krause, M.; Dunsch, L. *Angew. Chem., Int. Ed.* **2005**, *44* (10), 1557−1560.

(18) Yang, S. F.; Popov, A. A.; Kalbac, M.; Dunsch, L. *Chem.—Eur. J.* **2008**, *14* (7), 2084−2092.

(19) Chaur, M. N.; Melin, F.; Elliott, B.; Athans, A. J.; Walker, K.; Holloway, B. C.; Echegoyen, L. *J. Am. Chem. Soc.* **2007**, *129* (47), 14826−14829.

(20) Yang, S. F.; Kalbac, M.; Popov, A.; Dunsch, L. *ChemPhysChem* **2006**, *7* (9), 1990−1995.

(21) Chaur, M. N.; Aparicio-Angles, X.; Mercado, B. Q.; Elliott, B.; Rodriguez-Fortea, A.; Clotet, A.; Olmstead, M. M.; Balch, A. L.; Poblet, J. M.; Echegoyen, L. *J. Phys. Chem. C* **2010**, *114* (30), 13003−13009.

(22) Chaur, M. N.; Athans, A. J.; Echegoyen, L. *Tetrahedron* **2008**, *64* (50), 11387−11393.

(23) Feng, L.; Xu, J. X.; Shi, Z. J.; He, X. R.; Gu, Z. N. *Chem. J. Chin. Univ.* **2002**, *23* (6), 996−998.

(24) Zuo, T. M.; Beavers, C. M.; Duchamp, J. C.; Campbell, A.; Dorn, H. C.; Olmstead, M. M.; Balch, A. L. *J. Am. Chem. Soc.* **2007**, *129* (7), 2035−2043.

(25) Beavers, C. M.; Zuo, T. M.; Duchamp, J. C.; Harich, K.; Dorn, H. C.; Olmstead, M. M.; Balch, A. L. *J. Am. Chem. Soc.* **2006**, *128* (35), 11352−11353.

(26) Popov, A. A.; Krause, M.; Yang, S. F.; Wong, J.; Dunsch, L. *J. Phys. Chem. B* **2007**, *111* (13), 3363−3369.

(27) Yang, S.; Popov, A. A.; Dunsch, L. *J. Phys. Chem. B* **2007**, *111* (49), 13659−13663.

(28) Yang, S. F.; Troyanov, S. I.; Popov, A. A.; Krause, M.; Dunsch, L. *J. Am. Chem. Soc.* **2006**, *128* (51), 16733−16739.

(29) Yang, S. F.; Dunsch, L. *Chem.—Eur. J.* **2006**, *12* (2), 413−419.

(30) Yang, S. F.; Dunsch, L. *J. Phys. Chem. B* **2005**, *109* (25), 12320−12328.

(31) Yang, S. F.; Popov, A. A.; Dunsch, L. *Chem. Commun.* **2008**, 2885−2887.

(32) Wolf, M.; Muller, K. H.; Skourski, Y.; Eckert, D.; Georgi, P.; Krause, M.; Dunsch, L. *Angew. Chem., Int. Ed.* **2005**, *44* (21), 3306−3309.

(33) Zhang, Y.; Popov, A. A.; Schiemenz, S.; Dunsch, L. *Chem.—Eur. J.* **2012**, *18* (31), 9691−9698.

(34) Olmstead, M. M.; de Bettencourt-Dias, A.; Duchamp, J. C.; Stevenson, S.; Dorn, H. C.; Balch, A. L. *J. Am. Chem. Soc.* **2000**, *122* (49), 12220−12226.

(35) Krause, M.; Liu, X. J.; Wong, J.; Pichler, T.; Knupfer, M.; Dunsch, L. *J. Phys. Chem. A* **2005**, *109* (32), 7088−7093.

(36) Krause, M.; Wong, J.; Dunsch, L. *Chem.—Eur. J.* **2005**, *11* (2), 706−711.

(37) Zuo, T.; Walker, K.; Olmstead, M. M.; Melin, F.; Holloway, B. C.; Echegoyen, L.; Dorn, H. C.; Chaur, M. N.; Chancellor, C. J.; Beavers, C. M.; Balch, A. L.; Athans, A. J. *Chem. Commun.* **2008**, *9*, 1067−1069.

(38) Zuo, T.; Olmstead, M. M.; Beavers, C. M.; Balch, A. L.; Wang, G.; Yee, G. T.; Shu, C.; Xu, L.; Elliott, B.; Echegoyen, L.; Duchamp, J. C.; Dorn, H. C. *Inorg. Chem.* **2008**, *47* (12), 5234−5244.

(39) Stevenson, S.; Lee, H. M.; Olmstead, M. M.; Kozikowski, C.; Stevenson, P.; Balch, A. L. *Chem.—Eur. J* **2002**, *8* (19), 4528−4535.

(40) Yang, S.; Popov, A. A.; Chen, C.; Dunsch, L. *J. Phys. Chem. C* **2009**, *113* (18), 7616−7623.

(41) Yang, S.; Popov, A. A.; Dunsch, L. *Angew. Chem., Int. Ed.* **2008**, *47*, 8196−8200.

(42) Xu, W.; Wang, T.-S.; Wu, J.-Y.; Ma, Y.-H.; Zheng, J.-P.; Li, H.; Wang, B.; Jiang, L.; Shu, C.-Y.; Wang, C.-R. *J. Phys. Chem. C* **2011**, *115* (2), 402−405.

(43) Villaraza, A. J.; Bumb, A.; Brechbiel, M. W. *Chem. Rev.* **2010**, *110* (5), 2921−2959.

(44) Penfield, J. G.; Reilly, R. F. *Nat. Clin. Pract. Nephrol.* **2007**, *3* (12), 654−668.

(45) Caaravan, P.; Ellison, J. J.; McMurry, T. J.; Lauffer, R. B. *Chem. Rev.* **1999**, *99* (9), 2293−2352.

(46) Ersoy, H.; Rybicki, F. J. *J. Magn. Reson. Imaging* **2007**, *26* (5), 1190−1197.

(47) Bolskar, R. D.; Benedetto, A. F.; Husebo, L. O.; Price, R. E.; Jackson, E. F.; Wallace, S.; Wilson, L. J.; Alford, J. M. *J. Am. Chem. Soc.* **2003**, *125* (18), 5471−5478.

(48) Bolskar, R. D. Gadolinium Endohedral Metallofullerene-Based MRI Contrast Agents. In *Medicinal Chemistry and Pharmacological Potential of Fullerenes and Carbon Nanotubes*; Cataldo, F., Da Ros, T., Eds.; Springer: Amsterdam, The Netherlands, 2008; Vol. *1*, pp 157−180.
(49) Sitharaman, B.; Tran, L. A.; Pham, Q. P.; Bolskar, R. D.; Muthupillai, R.; Flamm, S. D.; Mikos, A. G.; Wilson, L. J. *Contrast Media Mol. Imaging* **2007**, *2* (3), 139−146.
(50) Toth, E.; Bolskar, R. D.; Borel, A.; Gonzalez, G.; Helm, L.; Merbach, A. E.; Sitharaman, B.; Wilson, L. J. *J. Am. Chem. Soc.* **2005**, *127* (2), 799−805.
(51) Zhang, J. F.; Fatouros, P. P.; Shu, C. Y.; Reid, J.; Owens, L. S.; Cai, T.; Gibson, H. W.; Long, G. L.; Corwin, F. D.; Chen, Z. J.; Dorn, H. C. *Bioconjugate Chem.* **2010**, *21* (4), 610−615.
(52) Shu, C.; Corwin, F. D.; Zhang, J.; Chen, Z.; Reid, J. E.; Sun, M.; Xu, W.; Sim, J. H.; Wang, C.; Fatouros, P. P.; Esker, A. R.; Gibson, H. W.; Dorn, H. C. *Bioconjugate Chem.* **2009**, *20* (6), 1186−1193.
(53) Laus, S.; Sitharaman, B.; Toth, E.; Bolskar, R. D.; Helm, L.; Wilson, L. J.; Merbach, A. E. *J. Phys. Chem. C* **2007**, *111* (15), 5633−5639.
(54) Sitharaman, B.; Wilson, L. J. *J. Biomed. Nanotechnol.* **2007**, *3*, 342−352.
(55) Sitharaman, B.; Bolskar, R. D.; Rusakova, I.; Wilson, L. J. *Nano Lett.* **2004**, *4* (12), 2373−2378.
(56) Mikawa, M.; Kato, H.; Okumura, M.; Narazaki, M.; Kanazawa, Y.; Miwa, N.; Shinohara, H. *Bioconjugate Chem.* **2001**, *12* (4), 510−514.
(57) Braun, K.; Dunsch, L.; Pipkorn, R.; Bock, M.; Baeuerle, T.; Yang, S. F.; Waldeck, W.; Wiessler, M. *Int. J. Med. Sci.* **2010**, *7* (3), 136−146.
(58) Fatouros, P. P.; Corwin, F. D.; Chen, Z. J.; Broaddus, W. C.; Tatum, J. L.; Kettenmann, B.; Ge, Z.; Gibson, H. W.; Russ, J. L.; Leonard, A. P.; Duchamp, J. C.; Dorn, H. C. *Radiology* **2006**, *240* (3), 756−764.
(59) Shu, C.-Y.; Ma, X.-Y.; Zhang, J.-F.; Corwin, F. D.; Sim, J. H.; Zhang, E.-Y.; Dorn, H. C.; Gibson, H. W.; Fatouros, P. P.; Wang, C.-R.; Fang, X.-H. *Bioconjugate Chem.* **2008**, *19* (3), 651−655.
(60) Shu, C.-Y.; Wang, C.-R.; Zhang, J.-F.; Gibson, H. W.; Dorn, H. C.; Corwin, F. D.; Fatouros, P. P.; Dennis, T. J. S. *Chem. Mater.* **2008**, *20* (6), 2106−2109.
(61) Svitova, A.; Braun, K.; Popov, A. A.; Dunsch, L. *ChemistryOpen* **2012**, *1* (5), 207−210.
(62) Popov, A. A.; Dunsch, L. *J. Am. Chem. Soc.* **2007**, *129* (38), 11835−11849.
(63) Chaur, M. N.; Valencia, R.; Rodriguez-Fortea, A.; Poblet, J. M.; Echegoyen, L. *Angew. Chem., Int. Ed.* **2009**, *48* (8), 1425−1428.
(64) Valencia, R.; Rodriguez-Fortea, A.; Clotet, A.; de Graaf, C.; Chaur, M. N.; Echegoyen, L.; Poblet, J. M. *Chem.—Eur. J.* **2009**, *15* (41), 10997−11009.
(65) Shinohara, H. *Rep. Prog. Phys.* **2000**, *63* (6), 843−892.
(66) Popov, A. A. *J. Comput. Theor. Nanosci.* **2009**, *6* (2), 292−317.
(67) Ma, Y.; Wang, T.; Wu, J.; Feng, Y.; Xu, W.; Jiang, L.; Zheng, J.; Shu, C.; Wang, C. *Nanoscale* **2011**, 3 (12), 4955−4957.
(68) Beavers, C. M.; Chaur, M. N.; Olmstead, M. M.; Echegoyen, L.; Balch, A. L. *J. Am. Chem. Soc.* **2009**, *131* (32), 11519−11524.
(69) Mercado, B. Q.; Beavers, C. M.; Olmstead, M. M.; Chaur, M. N.; Walker, K.; Holloway, B. C.; Echegoyen, L.; Balch, A. L. *J. Am. Chem. Soc.* **2008**, *130* (25), 7854−7855.
(70) Burke, B. G.; Chan, J.; Williams, K. A.; Ge, J. C.; Shu, C. Y.; Fu, W. J.; Dorn, H. C.; Kushmerick, J. G.; Puretzky, A. A.; Geohegan, D. B. *Phys. Rev. B* **2010**, *81* (11), 7.
(71) Fu, W.; Zhang, J.; Champion, H.; Fuhrer, T.; Azuremendi, H.; Zuo, T.; Zhang, J.; Harich, K.; Dorn, H. C. *Inorg. Chem.* **2011**, *50* (10), 4256−4259.
(72) Xu, L.; Li, S.-F.; Gan, L.-H.; Shu, C.-Y.; Wang, C.-R. *Chem. Phys. Lett.* **2012**, *521*, 81−85.
(73) Popov, A. A.; Dunsch, L. *J. Am. Chem. Soc.* **2008**, *130* (52), 17726−17742.
(74) Chen, N.; Zhang, E. Y.; Wang, C. R. *J. Phys. Chem. B* **2006**, *110* (27), 13322−13325.
(75) Tarabek, J.; Yang, S.; Dunsch, L. *ChemPhysChem* **2009**, *10* (7), 1037−1043.
(76) Laikov, D. N.; Ustynuk, Y. A. *Russ. Chem. Bull.* **2005**, *54* (3), 820−826.
(77) Laikov, D. N. *Chem. Phys. Lett.* **1997**, *281*, 151−156.
(78) Perdew, J. P.; Burke, K.; Ernzerhof, M. *Phys. Rev. Lett.* **1996**, *77* (18), 3865−3868.
(79) Laikov, D. N. An Implementation of the Scalar Relativistic Density Functional Theory for Molecular Calculations with Gaussian Basis Sets. *DFT2000 Satellite Symposium of the 10th International Congress of Quantum Chemistry*, Menton, France, 2000; p 43.
(80) Dyall, K. G. *J. Chem. Phys.* **1994**, *100* (3), 2118−2127.